World Electric Vehicle Journal

MDPI

*Article*

# Electric Vehicle Routing Problem with Drones Considering Weather Conditions and Time Windows

**Meiling He [1], Xi Yang [1], Xun Han [2,*], Jin Zhang [1], Xiaohui Wu [1] and Xiaolai Ma [3]**

[1] School of Automotive and Traffic Engineering, Jiangsu University, Zhenjiang 212013, China; hemeiling@ujs.edu.cn (M.H.); 2212304059@stmail.ujs.edu.cn (X.Y.); 2212304063@stmail.ujs.edu.cn (J.Z.); wuxiaohui@ujs.edu.cn (X.W.)
[2] Intelligent Policing Key Laboratory of Sichuan Province, Sichuan Police College, Luzhou 646000, China
[3] School of Transportation and Logistics, Southwest Jiaotong University, Chengdu 611756, China; maxiaolai@swjtu.edu.cn
* Correspondence: hanxun@scpolicec.edu.cn

**Abstract**

Inspired by the practical need for reliable drone-assisted logistics under varying weather conditions, this study investigates the vehicle–drone collaborative routing problem with weather constraints and time windows. The objective is to minimize the total delivery cost, including vehicle fixed costs, vehicle travel costs, drone flight costs, and time window penalty costs. To capture the impact of weather conditions on drone operations, a wind-speed-dependent dynamic flight speed function is introduced. A mathematical model is formulated, and an adaptive large neighborhood search algorithm integrated with genetic operations is proposed to enhance both local search efficiency and global exploration capability. Computational experiments on benchmark instances demonstrate that the proposed algorithm obtains high-quality solutions across different problem scales. Compared with the adaptive large neighborhood search algorithm and the improved genetic algorithm, the proposed approach reduces the optimal total delivery cost by an average of 4% and 2%, respectively. Sensitivity analysis further shows that increasing wind speed levels and the proportion of no-fly periods reduces the number of drone service tasks and increases total system cost, highlighting the significant impact of weather conditions on vehicle–drone collaborative delivery systems.

**Keywords:** logistics engineering; truck–drone collaborative delivery; adaptive large neighborhood search algorithm; weather conditions; time windows

Check for updates

Academic Editor: Aymeric Rousseau

Received: 23 March 2026
Revised: 24 April 2026
Accepted: 7 May 2026
Published: 8 May 2026

**Copyright:** © 2026 by the authors. Published by MDPI on behalf of the World Electric Vehicle Association. Licensee MDPI, Basel, Switzerland. This article is an open access article distributed under the terms and conditions of the Creative Commons Attribution (CC BY) license.

## 1. Introduction

In recent years, with the gradual improvement of low-altitude airspace management systems and the rapid development of intelligent logistics technologies, drone-based delivery has become an important component of modern logistics systems. Compared with traditional vehicle-only delivery modes, drones possess advantages such as high mobility, rapid response, and lower susceptibility to ground traffic congestion, which can improve the efficiency of last-mile distribution to a certain extent [1,2]. Particularly in rural and remote areas, where road density is relatively low, road conditions are often poor, and the geographical coverage is extensive, drones demonstrate clear advantages in traversing complex terrain and reducing transportation time. Therefore, they are widely regarded as an effective technological solution for addressing logistics distribution challenges in remote regions.

Meanwhile, driven by global carbon-neutrality goals and the development of green logistics, electric vehicles (EVs) have gradually become important delivery tools for logistics enterprises because of their low carbon emissions and high energy efficiency [3]. However, the limited battery capacity of EVs imposes additional constraints on delivery planning, as routing decisions must account not only for customer service requirements but also for vehicle energy feasibility. In this context, collaborative delivery systems integrating EVs and drones have attracted increasing attention from both academia and industry. In such systems, EVs undertake the primary ground transportation tasks and can also serve as launch and recovery platforms for drones, while drones exploit their operational flexibility to complete part of the last-mile delivery tasks. Through appropriate task allocation and coordinated route optimization, the EV–drone collaborative delivery mode has the potential to improve logistics efficiency and reduce overall operating costs.

Recent studies have extended EV–drone routing toward more realistic operational settings. For example, dynamic flight endurance has been incorporated into drone-assisted vehicle routing models [4]. More recent work has further considered time-dependent EV–drone routing with variable drone speeds and no-fly zones [5], while weather-aware drone delivery research has shown that uncertain wind conditions may substantially affect service reliability and scheduling feasibility [6]. These developments indicate that EV–drone collaborative routing is evolving from simplified launch-platform settings toward more integrated planning problems that better reflect practical delivery operations.

Despite these advances, the practical deployment of EV–drone collaborative delivery still faces substantial challenges. In particular, the safety and efficiency of drone flights are highly dependent on external environmental conditions, especially weather factors such as wind speed variations, rainfall, and temperature changes. These factors not only affect drone flight speed and energy consumption but may also create no-fly periods under adverse weather conditions. As a result, the feasible service area of drones and the collaborative operation mode between vehicles and drones may change dynamically, which further increases the complexity of the routing problem. Although recent studies have introduced weather information or no-fly restrictions into drone delivery and EV–drone routing, most of them focus on either robust drone scheduling or time-dependent routing extensions rather than jointly examining weather-dependent drone feasibility, EV routing, and customer time-window requirements within a unified optimization framework.

The main contributions of this paper are summarized as follows: (1) An EVRPDWTW model is formulated by jointly considering drone payload limits, flight energy consumption, wind-related operational effects, and no-fly period constraints. (2) A hybrid ALNS-GA solution approach is developed to efficiently solve the proposed problem. (3) The study provides a unified framework for analyzing EV routing, drone assignment, time-window constraints, and weather-aware collaborative delivery decisions.

The remainder of this paper is organized as follows. Section 2 reviews the related literature. Section 3 presents the problem formulation and mathematical model. Section 4 introduces the proposed algorithm. Section 5 validates the effectiveness of the model and algorithm using benchmark instances and sensitivity analyses. Section 6 concludes the paper and discusses future research directions.

## 2. Literature Review

This paper focuses on the vehicle–drone collaborative delivery routing problem considering weather conditions, with the objective of minimizing delivery cost. Based on a review of relevant literature, the discussion is organized into four aspects: electric vehicle routing problem, the vehicle–drone collaborative routing problem, routing problems considering weather conditions, and algorithm optimization.

### 2.1. Electric Vehicle Routing Problem

Driven by carbon-reduction policies and the transition toward sustainable urban logistics, the electric vehicle routing problem (EVRP) has become an important extension of the classical vehicle routing problem. Compared with conventional routing problems, EVRP must explicitly consider battery capacity, limited driving range, charging requirements, and the strong interaction between route design and energy feasibility. Consequently, the operational planning of electric fleets is not only a routing problem, but also an energy-constrained scheduling problem [7,8].

A foundational contribution in this field is the electric vehicle routing problem with time windows and recharging stations, in which customer service must be coordinated with battery limitations and recharging decisions. Since then, EVRP research has evolved in several directions. On the modeling side, scholars have extended the basic framework by incorporating heterogeneous fleets, partial recharging, battery swapping, and more realistic energy-consumption representations [9,10]. On the solution side, flexible variable neighborhood search frameworks have recently improved the capability of solving different EVRP variants under richer operational assumptions [8,11].

Recent literature also shows that EVRP research is shifting from simplified battery-feasibility settings toward more realistic operational environments. For example, realistic energy-consumption models that incorporate payload and vehicle speed have been introduced to better describe practical EV operations [12]. Load-dependent EVRP studies have further shown that the carried load may substantially affect energy consumption and route feasibility under time-window constraints [13]. In addition, time-dependent EVRP frameworks have incorporated congestion effects, variable travel times, and time-dependent battery discharge, thereby improving the realism of route planning in dynamic urban networks [14]. On the solution side, recent metaheuristic developments, such as flexible variable neighborhood search frameworks, have improved the capability of solving different EVRP variants under richer operational assumptions.

Overall, existing EVRP studies have established a solid foundation for energy-constrained routing and charging-related decision making. However, most of them focus on ground electric vehicle operations only. When drones are introduced into the delivery system, routing decisions must further account for launch-and-recovery coordination, task allocation between vehicles and drones, and additional operational feasibility constraints.

### 2.2. Vehicle Routing Problem with Drones

Drone-assisted routing has become an important research direction in last-mile logistics because it extends conventional vehicle routing to coordinated air–ground delivery systems. In VRPD, routing decisions must jointly consider customer assignment, vehicle–drone synchronization, and drone flight feasibility. Early studies mainly examined collaborative delivery modes and system operations. For example, Ham [15] studied an integrated scheduling problem with multiple trucks, drones, and depots under time-window constraints; Kitjacharoenchai et al. [16] proposed a two-echelon VRPD for last-mile delivery; and Huang et al. [17] developed an ant colony optimization algorithm for several VRPD variants. Although EVRPD studies have progressed in model formulation and algorithm design, some still regard electric vehicles mainly as drone launch platforms rather than active delivery units.

Subsequent studies enriched VRPD by introducing more realistic operational mechanisms and constraints. Some works modeled trucks as drone launch-and-recovery platforms and optimized coordinated air–ground routing accordingly [18,19]. Others incorporated payload-dependent drone endurance, no-fly zones, and pickup-and-delivery requirements into hybrid vehicle–drone systems [20,21]. In addition, time-dependent road travel

times and en-route synchronization have also been considered to better capture practical delivery processes [22,23]. These studies indicate that VRPD has evolved from simplified truck-assisted drone delivery toward more realistic collaborative routing settings with richer operational interactions.

On this basis, researchers have further extended truck–drone routing to electric vehicle–drone collaborative delivery. Early EVRPD studies mainly regarded electric vehicles as mobile carriers or "motherships" for drones and emphasized energy-efficient aerial delivery or memetic search for coordinated routing [24,25]. More recent work has begun to move beyond this simplified view by allowing EVs not only to serve as drone launch platforms, but also to undertake part of the ground delivery tasks. For example, Xiao et al. [26] investigated cooperative truck–drone delivery in rural regions with steep roads, while Zhang et al. [27] introduced customer time windows into electric vehicle–drone collaborative routing. Park et al. [28] further proposed a multi-modal electric logistics system in which electric trucks act as both delivery vehicles and floating chargers for electric drones. These studies suggest that EVs in collaborative delivery systems should no longer be treated merely as passive drone carriers; instead, they should be modeled as active decision units whose routing, energy use, and interaction with drones are jointly optimized.

Overall, existing drone-assisted and EV–drone routing studies have made substantial progress in modeling collaborative delivery structures, synchronization mechanisms, and operational constraints. However, most of them still assume relatively stable flight environments and pay limited attention to the role of external weather conditions in shaping drone feasibility, task allocation, and route coordination. This gap motivates the review of weather-aware routing studies in the following subsection.

### *2.3. Routing Problems Considering Weather Conditions*

In recent years, some studies have explicitly incorporated weather conditions into drone-assisted routing. Existing research shows that, compared with ground vehicles, drones are much more sensitive to environmental disturbances, and weather factors may directly affect flight speed, energy consumption, route feasibility, and service reliability. As a result, weather-aware routing has become an increasingly important extension of drone delivery research. Campuzano et al. [29] considered weather-dependent variable drone speeds, while Di Puglia Pugliese et al. [30] modeled uncertain energy consumption in truck–drone delivery. Dodge et al. [31] further incorporated wind speed, wind direction, payload, and uncertainty into a wind-affected drone–truck routing framework. These studies mainly focus on the continuous influence of weather on flight efficiency and energy use.

Another line of research emphasizes weather uncertainty and time-varying environmental impacts. Lu et al. [32] incorporated time-varying weather and time-window constraints into a synchronized vehicle–drone routing problem, while Cheng et al. [33] developed a robust drone delivery model with weather information to address service reliability under uncertain wind conditions. More recently, Ren et al. [34] extended EV–drone routing to a time-dependent setting with variable drone speeds and no-fly zones. These studies confirm that weather affects not only drone flight performance, but also route coordination and service scheduling.

Nevertheless, existing weather-aware routing studies still have two limitations. First, they mainly emphasize weather-related speed or energy effects, while explicit operational restrictions such as drone grounding are less often embedded in collaborative routing decisions. Second, limited attention has been paid to integrating weather-dependent drone feasibility with EV routing and customer time-window constraints in a single planning framework. To address this gap, this study investigates EVRPDWTW from a planning perspective and examines how weather conditions influence task allocation, route coor-

dination, and total delivery cost. This research gap also motivates the mapping of recent weather-aware routing studies, as summarized in Table 1.

**Table 1.** Comparison of routing studies considering weather.

| Reference | Vehicle–Drone Collaboration | Weather Factors | Weather Modeling | |
|---|---|---|---|---|
| | | | Speed | No-Fly |
| [28] | √ | Weather-dependent speed | √ | × |
| [29] | √ | Weather-related energy variation | × | × |
| [30] | √ | Wind speed, wind direction | √ | × |
| [31] | √ | Time-varying weather | √ | √ |
| [32] | × | Weather information, uncertain wind | √ | × |
| [33] | √ | Variable drone speed, no-fly zones | √ | √ |
| This paper | √ | Wind speed, wind direction, no-fly intervals | √ | √ |

Note: "√" indicates that the corresponding feature is considered in the study, while "×" indicates that it is not considered.

### 2.4. Algorithm of Vehicle Routing Problem with Drones

Regarding solution methodologies, most VRPD and its variants are addressed using heuristic or metaheuristic algorithms. Common approaches include genetic algorithms [35–37], ant colony optimization [38,39], and tabu search [40], which are well suited for handling the computational complexity of large-scale combinatorial optimization problems. Other researchers have adopted variable neighborhood search or adaptive large neighborhood search frameworks, enhancing solution efficiency through destroy-and-repair mechanisms [41–43]. As VRPD models continue to incorporate increasingly complex constraints, hybrid algorithms that combine genetic algorithms with local search or neighborhood-based strategies have gained attention [4,28,44], as they better balance global exploration capability and local solution refinement.

A comprehensive review of the existing literature leads to the following observations. First, existing EVRP studies have established a solid foundation for energy-constrained routing, but most of them focus on ground electric vehicle operations only. Second, research on drone-assisted and EV–drone collaborative routing has made substantial progress in modeling synchronization mechanisms and task allocation, yet some studies still treat electric vehicles mainly as drone launch platforms rather than active delivery units. Third, recent weather-aware routing studies have shown that wind speed, wind direction, and no-fly conditions may significantly affect drone feasibility and routing performance; however, relatively limited attention has been paid to their joint integration with EV routing and customer time-window constraints within a unified collaborative delivery framework. Fourth, for routing problems involving coupled constraints such as vehicle–drone coordination, time windows, energy limits, and weather-dependent feasibility, hybrid metaheuristic algorithms are more suitable for balancing global exploration and local exploitation.

Motivated by these observations, this study investigates the Electric Vehicle Routing Problem with Drones considering weather conditions and time windows (EVRPDWTW). The proposed model incorporates drone payload limitations, flight energy consumption, wind speed and wind direction effects, and no-fly period constraints. The objective is to minimize the total delivery cost, including vehicle fixed costs, vehicle travel costs, drone flight costs, and time-window penalty costs. To efficiently solve the problem, a hybrid heuristic algorithm combining Adaptive Large Neighborhood Search (ALNS) and a Genetic Algorithm (GA) is developed.

## 3. Description and Mathematical Model for EVRPDWTW

### 3.1. Problem Description

This paper investigates the electric vehicle–drone collaborative routing optimization problem considering weather conditions. The system consists of a distribution center and a fleet of electric vehicles, each equipped with a drone. Vehicles and drones collaboratively provide delivery services to customers with heterogeneous demands and soft time window constraints. During the delivery process, both vehicles and drones must satisfy payload capacity constraints; vehicles are additionally subject to battery capacity constraints, while drones must satisfy battery capacity and maximum flight distance limitations. Meanwhile, drone operations are affected by weather conditions: drones are prohibited from performing delivery tasks under hazardous weather conditions, and under allowable conditions the effects of wind speed and wind direction on flight speed are taken into account. By optimizing the cooperative routing and task allocation between vehicles and drones, all customer demands are fulfilled with the objective of minimizing the total delivery cost of the system. The collaborative delivery framework is illustrated in Figure 1.

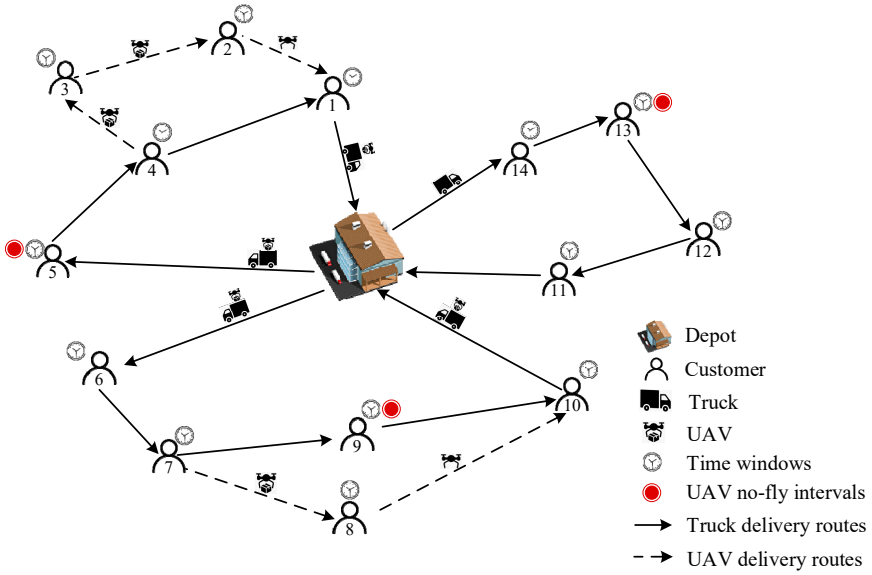



**Figure 1.** Schematic diagram of EVRPDWTW.

To facilitate the mathematical formulation of the EVRPDWTW, the following assumptions are adopted.

(1) A single distribution center is considered. All electric vehicles depart from the depot and must return to the same depot.
(2) Each electric vehicle is equipped with one dedicated drone, and each drone is launched from and recovered by its carrying vehicle.
(3) Each customer is served exactly once, either by an electric vehicle or by a drone, and customer demand cannot be split.
(4) The locations, demand quantities, and time-window information of all customers are known in advance. The demand of each customer does not exceed the vehicle capacity, and customers assigned to drones must also satisfy the drone payload limit.
(5) All electric vehicles and drones are assumed to be homogeneous, and their main operational parameters are known in advance.
(6) Each electric vehicle departs with a fully charged battery and must have sufficient energy to complete its route and return to the depot. Vehicle charging or battery swapping during delivery is not considered.

(7) A drone may serve multiple customers in one flight mission, subject to payload, battery, flight-distance, and synchronization constraints, and must return to its carrying vehicle after completing the mission.
(8) Road traffic conditions are assumed to be deterministic, and electric vehicles travel at a constant speed without considering congestion, road closures, or other stochastic disturbances.
(9) Customer time windows are soft. Early or late service is allowed, but the corresponding penalty cost is incurred.
(10) Weather conditions are modeled in a time-dependent deterministic manner, as described in Section 3.2. During no-fly intervals, drone operations are prohibited; during flyable intervals, wind conditions affect drone flight speed and feasibility.
(11) For tractability, real-time route updates and detailed aerodynamic or energy-consumption effects are not explicitly considered.

### *3.2. Effects of Weather Conditions*

In practical last-mile delivery operations, weather conditions, especially wind variations, may significantly affect drone flight safety, travel time, and route feasibility. Following existing weather-aware routing studies [29,31], this study adopts a time-dependent weather representation to incorporate these effects into the EVRPDWTW framework.

(1) Flight constraints under no-fly weather conditions

Let the planning horizon be partitioned into intervals $[\tau_r, \tau_{r+1}), r \in R$. For each interval $r$, the weather state is characterized by a binary no-fly variable $\rho_r$, wind speed $v_r^w$ and wind direction $\theta_r^w$. If a drone departs during interval $r$, the corresponding weather parameters of that interval are used to determine its flight feasibility and travel speed. This piecewise-constant setting allows the model to capture temporal weather variation without introducing excessive computational complexity.

It should be noted that adverse meteorological phenomena, such as heavy rain, snowfall, hail, lightning, and low visibility, are not explicitly modeled as separate continuous weather variables in this study. Instead, their operational effect is aggregated into the binary no-fly indicator $\rho_r$. When $\rho_r = 1$, drone takeoff is prohibited in interval $r$, and all delivery tasks scheduled in that interval must be served by ground vehicles. When $\rho_r = 0$ drone operations are allowed, and the flight state is further affected by the wind speed and wind direction in the corresponding interval.

(2) Drone flight speed under wind influence

When a drone performs a delivery task under wind field conditions, its effective ground speed is determined by the vector synthesis of its nominal cruising speed and the wind velocity. As illustrated in Figure 2, the flight speed under wind influence $v_h$ is the vector sum of its nominal cruising speed $v_a$ and the wind speed $v_r^w$. In Equation (1) $\psi_{ij}$, denotes the direction angle of the drone flying from node $i$ to node $j$, and $\delta_{ij}$ represents the yaw angle. In Equation (2) $\vec{u}$, denotes the unit vector of the drone flight direction, while $\vec{n}$ represents the unit vector of the trajectory direction from node $i$ to node $j$.

The weather representation adopted in this study is intended for planning-level routing optimization. To balance realism and solvability, weather conditions are modeled as deterministic and piecewise constant over time. The current framework does not explicitly consider stochastic weather evolution, turbulence, nonlinear aerodynamic drag, or real-time weather updates. These factors may influence drone energy consumption and route execution in practice and will be incorporated in future research through stochastic and dynamic weather-aware routing models.

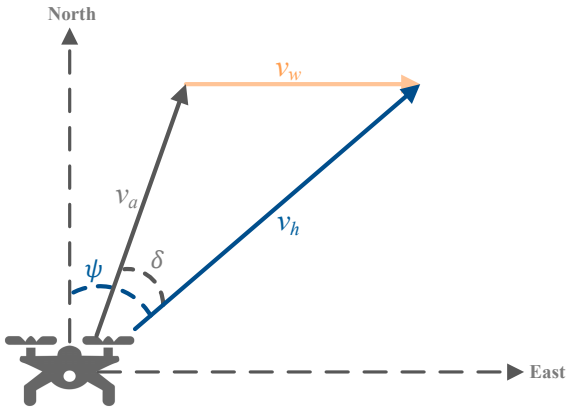



**Figure 2.** Illustration of drone flight speed under wind influence.

$$v_h = \sqrt{v_a^2 + v_r^{w2} - 2v_a v_r^w \cos\left(\frac{\pi(\psi_{ij} - \theta_r^w + \delta_{ij})}{180^\circ}\right)} \quad \forall (i,j) \in A \tag{1}$$

$$\psi_{ij} = \left(\frac{180^\circ}{\pi}\right) \cdot \arccos\left(\frac{\vec{u} \cdot \vec{n}}{\left|\vec{u}\right| \cdot \left|\vec{n}\right|}\right) \quad \forall (i,j) \in A \tag{2}$$

$$\delta_{ij} = \left(\frac{180^\circ}{\pi}\right) \cdot \arcsin\left(\frac{v_r^w}{v_a} \cdot \sin\left(\frac{\pi(\theta_r^w - \psi_{ij})}{180^\circ}\right)\right) \quad \forall (i,j) \in A \tag{3}$$

### *3.3. Mathematical Model for EVRPDWTW*

The symbols and their corresponding definitions used in the mathematical model are presented in Tables 2–4.

**Table 2.** Sets of EVRPDWTW model.

| Set | Description |
|---|---|
| $N$ | Set of customer nodes, $N = \{1, 2, \ldots, n\}$ |
| $K$ | Set of vehicles, $K = \{1, 2, \ldots, k\}$ |
| $H$ | Set of drones, $H = \{1, 2, \ldots, h\}$ |
| $R$ | Set of weather intervals, $R = \{1, 2, \ldots, r\}$ |

**Table 3.** Parameters of EVRPDWTW model.

| Parameter | Description |
|---|---|
| $C_1$ | Fixed dispatch cost per vehicle |
| $C^K$ | Vehicle transportation cost per unit time |
| $C^D$ | drone transportation cost per unit time |
| $d_i$ | Demand of customer $i$ |
| $Q_k$ | Maximum payload capacity of vehicle $k$ |
| $Q_h$ | Maximum payload capacity of drone $h$ |
| $v_k$ | Traveling speed of vehicle $k$ |
| $S_{\max}$ | Maximum flight distance of a drone |
| $E_i$ | Earliest service time of customer $i$ |
| $L_i$ | Latest service time of customer $i$ |
| $f$ | Penalty coefficient for early service |
| $e$ | Penalty coefficient for late service |
| $\sigma_i$ | Service duration required at customer $i$ |
| $s_{ij}$ | Distance between customer $i$ and customer $j$ |

**Table 3.** *Cont.*

| Parameter | Description |
|---|---|
| $t_{ij}^k$ | Travel time of vehicle $k$ from customer $i$ to customer $j$ |
| $t_{ij}^h$ | Travel time of drone $h$ from customer $i$ to customer $j$ |
| $t_{io}^h$ | Travel time of drone $h$ from customer $i$ to node $o$ |
| $t_{oj}^h$ | Travel time of drone $h$ from node $o$ to customer $j$ |
| $t_i^k$ | Arrival time of vehicle $k$ at customer $i$ |
| $t_i^h$ | Arrival time of drone $h$ at customer $i$ |
| $E_i^k$ | Remaining energy of vehicle $k$ upon arrival at node $i$ |
| $E_{\max}^k$ | Maximum energy capacity of vehicle $k$ |
| $E_{\max}^h$ | Maximum energy capacity of drone |
| $\eta$ | Energy consumption coefficient per unit distance for vehicles |
| $C_w$ | Payload-related energy consumption coefficient |
| $C_v$ | Speed-related energy consumption coefficient |
| $E(v_h, q_h)$ | Energy consumption of drone $h$ at speed $v_h$ with payload $q_h$ |
| $T_h^{re}$ | Time for drone $h$ to return to the vehicle, $h \in H$ |
| $T_{ih}$ | Departure time of drone $h$ from customer $i$ |
| $W^{\max}$ | Maximum waiting time of a drone at the recovery point |

**Table 4.** Decision variables of the EVRPDWTW model.

| Variable | Description |
|---|---|
| $x_{ij}^k$ | Binary variable equal to 1 if vehicle $k$ travels from customer $i$ to customer $j$, 0 otherwise |
| $x_{0j}^k$ | Binary variable equal to 1 if vehicle $k$ travels from the depot to customer $j$, 0 otherwise |
| $x_{i0}^k$ | Binary variable equal to 1 if vehicle $k$ travels from the customer $i$ to the depot, 0 otherwise |
| $y_{ij}^h$ | Binary variable equal to 1 if drone $h$ travels from customer $i$ to customer $j$, 0 otherwise |
| $B_{ir}$ | Binary indicator equal to 1 if the drone service associated with customer $i$ is executed during interval $r$, and 0 otherwise |

The mathematical model of EVRPDWTW is formulated as a mixed-integer program. The overall objective function consists of four components, fixed vehicle dispatch cost $Z_1$, vehicle transportation cost $Z_2$, drone transportation cost $Z_3$, and time-window penalty cost $Z_4$, and is formulated as follows:

$$\min Z = Z_1 + Z_2 + Z_3 + Z_4 \tag{4}$$

$$Z_1 = C_1 \sum_{j \in N} \sum_{k \in K} x_{0j}^k \tag{5}$$

$$Z_2 = C^K \sum_{i,j \in N} \sum_{k \in K} t_{ij}^k x_{ij}^k \tag{6}$$

$$Z_3 = C^D \sum_{i,j \in N} \sum_{h \in H} t_{ij}^h y_{ij}^h \tag{7}$$

$$\begin{aligned} Z_4 = & \sum_{k \in K} \sum_{i \in N} \left( f\max(E_i - t_i^k, 0) + e\max(t_i^k - L_i, 0) \right) + \\ & \sum_{h \in H} \sum_{i \in N} \left( f\max(E_i - t_i^h, 0) + e\max(t_i^h - L_i, 0) \right) \end{aligned} \tag{8}$$

subject to

$$\sum_{k=1}^{K} x_{ij}^{k} + \sum_{h=1}^{H} y_{ij}^{h} = 1, \quad \forall i, j \in N \tag{9}$$

$$\sum_{i,j \in N} d_j x_{ij}^{k} \le Q_k, \quad \forall k \in K \tag{10}$$

$$d_j y_{ij}^{h} \le Q_h, \quad \forall i, j \in N, h \in H \tag{11}$$

$$t_i^k + t_{ij}^k + \sigma_i \le t_j^k, \quad t_i^h + t_{ij}^h + \sigma_i \le t_j^h, \quad \forall i, j \in N \tag{12}$$

$$y_{ij}^{h} \le 1 - \sum_{r \in R} B_{ir} \rho_r, \quad \forall i, j \in N, \forall h \in H \tag{13}$$

$$\sum_{j=1}^{N} x_{0j}^{k} \le 1, \quad \forall k \in K \tag{14}$$

$$\sum_{i=1}^{N} x_{i0}^{k} \le 1, \quad \forall k \in K \tag{15}$$

$$E_0^k = E_{\max}^k, \quad \forall k \in K \tag{16}$$

$$E_j^k \le E_i^k - \eta d_{ij} + M\left(1 - x_{ij}^{k}\right), \quad \forall i, j \in N, k \in K \tag{17}$$

$$0 \le E_i^k \le E_{\max}^k, \quad \forall i \in N, k \in K \tag{18}$$

$$E_i^k \ge \eta s_{i0}, \forall i \in N, k \in K \tag{19}$$

$$\sum_{j=0, j \ne i}^{N} x_{ij}^{k} = \sum_{j=0, j \ne i}^{N} x_{ji}^{k}, \quad \forall i \in N, \quad \forall k \in K \tag{20}$$

$$\sum_{j=0, j \ne i}^{N} y_{ij}^{h} = \sum_{j=0, j \ne i}^{N} y_{ji}^{h}, \quad \forall i \in N, \quad \forall h \in H \tag{21}$$

$$t_{ij}^{k} = \frac{s_{ij}}{v_k}, \quad t_{ij}^{h} = \frac{s_{ij}}{v_h}, \quad \forall i, j \in N \tag{22}$$

$$\sum_{i=1}^{N} \sum_{j=1}^{N} s_{ij} y_{ij}^{h} \le S_{\max}, \quad \forall h \in H \tag{23}$$

$$E(v_h, q_h) = C_v \cdot v_h^2 + C_w \cdot q_h \tag{24}$$

$$\sum_{i=1}^{N} \sum_{j=1}^{N} E(v_h, q_h) \cdot y_{ij}^{h} \le E_{\max}^{h}, \quad \forall h \in H \tag{25}$$

$$T_h^{re} = T_{ih} + t_{io}^{h} + t_{oj}^{h}, \quad \forall i, o, j \in N, \forall h \in H \tag{26}$$

$$T_r \le T_{jk}, \quad \forall h \in H, \forall k \in K \tag{27}$$

$$0 \le T_{jk} - T_r \le W^{\max}, \quad \forall h \in H, \forall k \in K \tag{28}$$

Equation (4) defines the objective function, which minimizes the total delivery cost, including the fixed dispatch cost of electric vehicles, the transportation costs of electric vehicles and drones, and the penalty costs associated with time window violations. Equation (9) ensures that each customer is served exactly once, either by an electric vehicle or by a drone. Equations (10) and (11) impose payload capacity constraints, requiring that the delivery load of each vehicle and drone does not exceed its maximum carrying capacity. Equation (12) enforces the time window constraints for both vehicles and drones, ensuring that the service start time at each customer lies between the earliest and latest allowable

service times; penalties are incurred in cases of early or late service. Equation (13) represents the no-fly weather constraint, under which drone operations are prohibited during adverse weather conditions. Equations (14) and (15) require that each vehicle departs from and returns to the depot. Equation (16) ensures that all electric vehicles depart from the distribution center with a fully charged battery. Equations (17) and (18) impose energy constraints on electric vehicles. Equation (19) guarantees that, after completing service at the current node, each vehicle retains sufficient remaining energy to return to the depot. Equations (20) and (21) describe the flow conservation constraints for vehicle and drone routes. Equation (22) calculates the travel time of vehicles and drones between customer nodes.

Equations (23)–(26) define the drone coordination constraints: Equation (23) limits the total drone flight distance to its maximum allowable range, while Equations (24) and (25) ensure that the energy consumption of the drone along each flight segment does not exceed its battery capacity. Equation (26) computes the drone return time. Equation (27) requires that the drone completes its task and arrives at the recovery point no later than the corresponding vehicle arrival time. Finally, Equation (28) limits the maximum waiting time of a drone after arriving at the recovery point before being retrieved by the vehicle.

## 4. ALNS-GA for EVRPDWTW

Due to the coupled effects of time windows, no-fly weather intervals, vehicle energy limits, and vehicle–drone synchronization, the EVRPDWTW exhibits a highly fragmented feasible search space. A single search strategy is therefore likely to suffer from either premature convergence or insufficient local exploitation. To address this issue, this study develops a hybrid ALNS-GA framework, in which ALNS is used to perform large-scale solution destruction and reconstruction for intensive neighborhood exploration, while GA-based crossover and mutation are employed to maintain population diversity and enhance global exploration. In this way, the proposed framework balances intensification and diversification in solving the EVRPDWTW. The flowchart of the proposed ALNS-GA framework is shown in Figure 3.

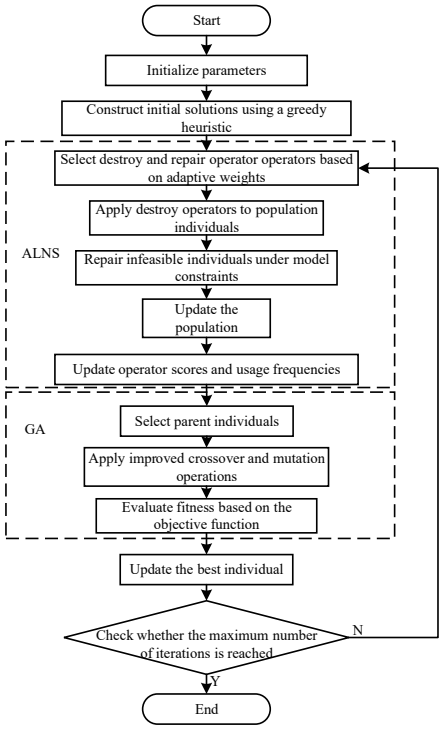



**Figure 3.** Flowchart of ALNS-GA.

During each iteration, the fitness of each individual is evaluated according to the objective function in Equations (4)–(8), while infeasible solutions are repaired with respect to the routing, time-window, no-fly weather, energy, and synchronization constraints in Equations (9)–(24).

### *4.1. Initial Solution Construction*

To improve solution quality in the initial stage of the algorithm, a greedy initialization strategy based on distance-related heuristics is developed. On the basis of random initialization, a greedy construction mechanism is incorporated to ensure both the quality and diversity of the initial solutions.

First, a distance-based heuristic factor matrix is constructed as $\eta_{ij} = d_{ij}^{-\beta}$ which characterizes the relative attractiveness between customer nodes. An $\varepsilon$ greedy strategy is introduced to balance greedy construction and random initialization. Under this strategy, a portion of individuals are still generated using random routing, while greedy construction is applied to the remaining individuals with a certain probability. The basic procedure is as follows:

(1) A starting node is randomly selected from the candidate node set;
(2) At each iteration, the next service node is selected from the set of unvisited nodes according to one of the following two strategies: Greedy selection: $(1-\varepsilon)$ the next node is determined based on the maximum attractiveness (i.e., the shortest distance); Randomized selection $(\varepsilon)$: roulette-wheel selection is performed based on the normalized attractiveness values;
(3) The above process is repeated until a complete route is constructed.

### *4.2. ALNS Algorithm*

#### 4.2.1. Adaptive Operator Weight Updating Mechanism

In the ALNS phase, destroy and repair operators are selected by roulette wheel according to adaptive weights. After the selected operators are applied to an individual, the generated solution is evaluated and accepted or rejected according to its objective value and feasibility. The weights are then updated based on the operator's historical contribution, so that operators producing high-quality solutions are more likely to be selected in subsequent iterations.

The adaptive update rule for operator weights is defined as follows:

$$w_i^{(t+1)} = (1-\lambda) \cdot w_i^{(t)} + \lambda \cdot \frac{s_i}{c_i} \tag{29}$$

Here, $w_i^{(t)}$ denotes the weight of operator at iteration, $s_i$ represents the score assigned to operator $i$ in the current iteration, and $c_i$ denotes the cumulative number of times that operator $i$ has been selected. The parameter $\lambda \in (0,1)$ is the learning rate, which controls the magnitude of the weight update.

The operator scoring rules are defined as follows. If the new solution improves the current solution, the current solution is replaced. If it also improves the global best solution found so far, the selected operator is assigned the highest score ($s_1$); otherwise, the operator receives the second-highest score ($s_2$). If the new solution does not improve the current solution but is still accepted according to the acceptance criterion, the operator receives a medium score ($s_3$). If the new solution is rejected, the current solution remains unchanged, and the operator receives the lowest score ($s_4$).

#### 4.2.2. Destroy Operators

Three destroy operators are employed in the ALNS phase, namely random destroy, consecutive destroy, and cost-based greedy destroy. Their common purpose is to remove a subset of customer tasks from the current solution and create room for subsequent reconstruction under the EVRPDWTW constraints.

(1) Random Destroy Operator

A subset of customer nodes is randomly selected and removed from the current solution. If a removed node corresponds to a drone launch or recovery point, the associated drone-served customer is removed simultaneously. Since a vehicle-served node may also act as a drone launch or recovery point, the removal of one customer may trigger the removal of additional related tasks.

(2) Consecutive Destroy Operator

A starting position is randomly selected on the current vehicle route, and a consecutive sequence of customer nodes is removed as a sub-route. Similar to the random destroy operator, if any removed node serves as a drone launch or recovery point, the corresponding drone task is removed simultaneously to maintain route consistency and avoid infeasible coordination relationships.

(3) Greedy Destroy Operator

This operator removes customer nodes associated with route segments having relatively high total costs. For each segment in the current solution, the route cost is evaluated according to the service mode. If the customer is served by a vehicle, the corresponding vehicle travel cost is computed; if the customer is served by a drone, the drone flight cost from the launch point to the customer and from the customer to the recovery point is evaluated. Several customer nodes associated with the highest-cost segments are then removed to create greater opportunities for subsequent improvement.

#### 4.2.3. Repair Operators

Two repair operators are used to reconstruct the partial solution, namely random repair and greedy repair. For each removed customer, candidate insertion positions are checked against vehicle/drone capacity, time-window, no-fly, energy, and synchronization constraints. Feasible insertions are then executed either randomly or according to the minimum objective increase.

(1) Random repair operator

For each customer node removed during the destroy phase, the algorithm randomly inserts it into a feasible position in the current solution, without distinguishing between vehicle routes and drone routes. If the insertion occurs in a vehicle route, the vehicle capacity and time window constraints must be satisfied. If the insertion occurs in a drone route, the constraints related to flight range, payload capacity, and no-fly time windows must also be satisfied.

(2) Greedy repair operator

All feasible insertion positions in the current solution are enumerated. Each removed customer node is temporarily inserted into these positions to generate candidate solutions, which are then evaluated using the objective function. The insertion position that results in the minimum objective value is selected for the actual insertion.

For the vehicle–drone collaborative routing problem, several insertion scenarios are considered, including inserting a new drone task, inserting into an existing drone route,

and inserting into a vehicle route. All insertions must satisfy the corresponding vehicle or drone feasibility conditions.

### *4.3. Genetic Operations*

#### 4.3.1. Crossover Operation

A crossover operator based on local inversion perturbation is employed to reorganize route structures while preserving useful genetic information from existing individuals. For a selected individual, a gene position $G_1$ is first randomly chosen, and a random number $p \in [0, 1]$ is generated. If $p$ is smaller than the crossover probability threshold, another gene position $G_2$ is randomly selected from the same individual. Otherwise, another chromosome is randomly selected from the population, and the neighboring gene position corresponding to $G_1$ in that chromosome is identified; the corresponding position in the current individual is then used as $G_2$.

A local inversion operation is subsequently performed on the segment between $G_1$ and $G_2$, thereby generating a new offspring. This operator preserves part of the original route structure while introducing local reordering, which helps improve information exchange between individuals without excessively disrupting promising routing patterns.

#### 4.3.2. Mutation Operation

A mutation operator based on segment inversion is adopted to enhance population diversity and help the search escape local optima. Once mutation is triggered, a route segment is randomly selected and inverted to reconstruct the individual. The mutated solution is then checked for feasibility and repaired if necessary under the EVRPDWTW constraints.

## 5. Experimental Results and Analysis

Since no publicly available benchmark instances exist for the EVRPDWTW problem, this study extends the VRPD benchmark instances reported by Sacramento [45] to construct EVRPDWTW test instances. The original instances provide customer coordinates, demand information, and basic collaborative delivery structures, which makes them suitable for evaluating the proposed vehicle–drone routing framework. On this basis, additional attributes related to time windows, weather conditions, and EV/drone operational constraints are introduced.

Specifically, customer time windows and depot operating hours are added to the original instances, and the depot operating time window is set from 8:00 to 18:00. The planning horizon is further divided into multiple intervals, each of which is assigned a predefined weather state, including a no-fly indicator, wind speed, and wind direction. Through this extension, the original static VRPD instances are transformed into weather-aware EVRPDWTW instances that can be used to validate the proposed model under time-window-constrained collaborative delivery scenarios.

The number of available vehicles and drones at the depot is assumed to be sufficient. Small-scale instances contain 6, 10, and 20 customers, whereas medium- and large-scale instances range from 50 to 200 customers. This setting allows the scalability of the proposed algorithm to be examined under different problem sizes.

The main operational parameters are referenced from Sacramento [45]. The vehicle capacity is set to 1400 kg, with an average speed of 15 m/s and a transportation cost $C^K$ of 0.58 CNY/min. The drone capacity is 5 kg, with a nominal cruising speed of 22 m/s. The drone launch time, recovery time, and service time are each set to 1 min, and the maximum waiting time at the recovery point is set to 10 min. The drone transportation cost is assumed to be 10% of the vehicle transportation cost $C^D$, i.e., 0.058 CNY/min. For

computational consistency, all speed-related parameters are converted into a common unit in the implementation.

Although the extended instances are not derived from real-world logistics data, they provide a structured and reproducible testbed for evaluating the proposed model and analyzing the effects of weather on drone feasibility and route coordination.

After extensive experimental testing, the algorithm parameters are configured as follows. The maximum number of iterations is set to 2000. In the ALNS framework, the selection of destroy and repair operators follows an adaptive probability mechanism, where the selection probabilities depend on the historical performance of the operators. Let $w_d$ and $w_r$ denote the weights of destroy and repair operators, respectively; $c_d$ and $c_r$ denote the number of times the corresponding operators are used; and $s_d$ and $s_r$ represent the accumulated scores of the operators.

At initialization, the weights of all operators are set to uniform vectors, i.e., $w_d = (1,1,1)$ and $w_r = (1,1)$, indicating that all operators have equal selection probabilities. The usage count and score vectors are initialized to zero, i.e., $c_d = (0,0,0)$, $c_r = (0,0)$, $s_d = (0,0,0)$ and $s_r = (0,0)$.

In each iteration, the selected operators receive corresponding reward scores based on the quality of the generated solution. The reward levels are drawn from the discrete set $\{0.5, 0.8, 1.2, 1.5\}$, corresponding to the cases where a solution is accepted but inferior, accepted with improvement, reaches the current best solution, and updates the global best solution, respectively. By updating the accumulated scores and usage counts of the operators, their weights are adaptively adjusted over the iterations.

In the genetic operations, the crossover probability and mutation probability are set to 0.6 and 0.1, respectively. The parameter settings are determined based on related EV–drone routing literature [25] and preliminary computational experiments. The algorithm is implemented in MATLAB R2022b and executed on a system equipped with an Intel(R) Core(TM) Ultra 7255H processor (2.00 GHz) running the Windows 11 operating system.

To characterize the dynamic impact of weather conditions on drone operations in the computational experiments, this study adopts a time-dependent weather representation in which each time interval is associated with wind speed, wind direction, and no-fly status. Different time intervals may correspond to different weather states, thereby capturing the temporal variation in the operating environment. According to drone manufacturer specifications and relevant studies [46,47], drone flight performance is highly sensitive to wind conditions, and its flight speed, energy consumption, and operational safety may vary substantially with wind intensity. For experimental analysis, the weather conditions are classified into three categories: ideal weather (0–4 m/s), flight-restricted weather (4–8 m/s), and no-fly weather (>8 m/s).

### *5.1. Algorithm Effectiveness Validation*

To evaluate the effectiveness of ALNS-GA for solving the VRPD, a set of classical benchmark instances from the literature is used for computational experiments. Table 5 compares ALNS-GA with the adaptive large neighborhood search (ALNS) proposed by Sacramento [45], the adaptive ant colony optimization (AACO) proposed by Stodola [48], and the hybrid genetic algorithm (HGA) developed by Euchi [35], all tested under identical experimental conditions. The columns "ALNS [45]", "HGA [35]", "AACO [48]", and "ALNS-GA" report the average total delivery cost over 10 independent runs, while "SD" denotes the standard deviation of the ALNS-GA results.

**Table 5.** Comparison of VRPD case study solution results.

| Instance | Customers | Vehicles | ALNS [45] | HGA [35] | AACO [48] | ALNS-GA | SD |
|---|---|---|---|---|---|---|---|
| 6.5.1 | 6 | 1 | 1.10 | 1.10 | 1.10 | 1.1 | 0.00 |
| 6.5.2 | 6 | 1 | 0.84 | 0.84 | 0.84 | 0.84 | 0.00 |
| 6.5.3 | 6 | 1 | 1.21 | 1.21 | 1.21 | 1.21 | 0.00 |
| 6.5.4 | 6 | 1 | 0.95 | 0.95 | 0.95 | 0.95 | 0.00 |
| 10.5.1 | 10 | 1 | 1.66 | 1.66 | 1.66 | 1.66 | 0.00 |
| 10.5.2 | 10 | 1 | 1.45 | 1.45 | 1.45 | 1.45 | 0.00 |
| 10.5.3 | 10 | 1 | 1.47 | 1.47 | 1.47 | 1.47 | 0.00 |
| 10.5.4 | 10 | 1 | 1.28 | 1.28 | 1.28 | 1.28 | 0.00 |
| 20.10.1 | 20 | 1 | 3.25 | 2.98 | 3.25 | 3.25 | 0.00 |
| 20.10.2 | 20 | 1 | 3.09 | 3.06 | 3.09 | 3.09 | 0.00 |
| 20.10.3 | 20 | 1 | 3.70 | 3.30 | 3.30 | 3.7 | 0.00 |
| 20.10.4 | 20 | 1 | 3.31 | 3.2 | 3.32 | 3.2 | 0.00 |
| 50.10.1 | 50 | 1 | 5.86 | 5.73 | 5.86 | 5.86 | 0.00 |
| 50.10.2 | 50 | 1 | 5.58 | 5.44 | 5.56 | 5.58 | 0.02 |
| 50.10.3 | 50 | 1 | 5.42 | 5.18 | 5.59 | 5.59 | 0.10 |
| 50.10.4 | 50 | 1 | 5.21 | 5.07 | 5.15 | 5.14 | 0.09 |
| 100.40.1 | 100 | 2 | 29.14 | 29.14 | 29.02 | 28.19 | 0.16 |
| 100.40.2 | 100 | 2 | 30.99 | 30.36 | 30.35 | 30.35 | 0.05 |
| 100.40.3 | 100 | 2 | 29.02 | 29.01 | 29.01 | 28.71 | 0.23 |
| 100.40.4 | 100 | 2 | 28.97 | 28.59 | 28.57 | 28.46 | 0.13 |
| 150.20.1 | 150 | 2 | 17.32 | 17.32 | 17.32 | 16.9 | 0.62 |
| 150.20.2 | 150 | 2 | 16.63 | 16.63 | 16.63 | 17.46 | 0.51 |
| 150.20.3 | 150 | 2 | 17.41 | 17.41 | 17.67 | 17.7 | 0.14 |
| 150.20.4 | 150 | 2 | 16.88 | 16.88 | 16.89 | 16.89 | 0.71 |
| 200.20.1 | 200 | 2 | 21.22 | 21.22 | 21.00 | 20.92 | 0.67 |
| 200.20.2 | 200 | 2 | 21.46 | 21.46 | 21.45 | 21.86 | 0.27 |
| 200.20.3 | 200 | 2 | 20.85 | 20.85 | 21.01 | 21.11 | 0.12 |
| 200.20.4 | 200 | 2 | 19.23 | 19.23 | 19.24 | 19.85 | 0.13 |
| | avg | | 11.23 | 11.14 | 11.19 | 11.21 | 0.25 |

The results indicate that for small-scale instances (6–20 customers), ALNS-GA consistently matches the known best solutions. For medium- and large-scale instances (50–200 customers), it maintains high stability and achieves solution quality close to the best known results. The SD values are generally small, with an average of 0.25, indicating limited fluctuation across repeated runs and thus good robustness. Among the 28 benchmark instances, ALNS-GA obtains the best known or improved solutions in 21 cases. In several instances, the total delivery cost is further reduced compared with the reference algorithms, with a maximum improvement of 3.39%. Overall, the results confirm that ALNS-GA can solve the VRPD efficiently and robustly.

### *5.2. EVRPDWTW Instance Analysis*

To evaluate the performance of ALNS-GA on the EVRPDWTW, 28 benchmark instances are used for comparison with ALNS [45] and CAGA [49]. A baseline weather setting is adopted, in which the drone no-fly period is set to 10:00–12:00 and the wind speed in the remaining periods is kept within Beaufort scale level 3 or lower. Table 6 reports the average results of the three algorithms over 10 independent runs under identical parameter settings and stopping criteria.

**Table 6.** Comparison of EVRPDWTW case study solution results.

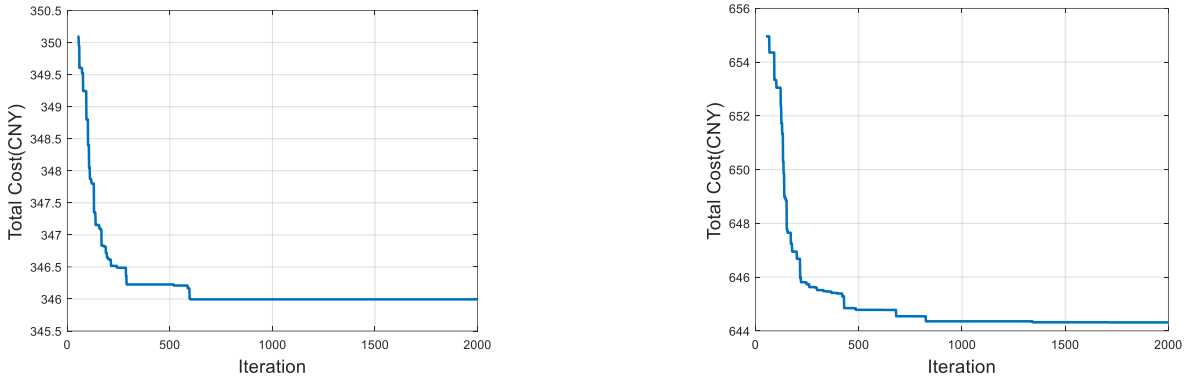
| Instance | Customers | BKS | ALNS-GA | ALNS [45] | $gap_{ALNS}$ (%) | CAGA [49] | $gap_{GA}$ (%) |
|---|---|---|---|---|---|---|---|
| Cr601 | 6 | 305.21 | 305.21 | 305.21 | 0.00% | 305.21 | 0.00% |
| Cr602 | 6 | 304.14 | 304.14 | 304.14 | 0.00% | 304.14 | 0.00% |
| Cr603 | 6 | 303.15 | 303.15 | 303.15 | 0.00% | 303.15 | 0.00% |
| Cr604 | 6 | 307.02 | 307.02 | 309.37 | −0.76% | 307.02 | 0.00% |
| Cr101 | 10 | 308.06 | 308.06 | 308.06 | 0.00% | 308.06 | 0.00% |
| Cr102 | 10 | 305.56 | 305.56 | 306.78 | −0.40% | 307.34 | −0.58% |
| Cr103 | 10 | 308.39 | 308.39 | 308.39 | 0.00% | 308.39 | 0.00% |
| Cr104 | 10 | 306.36 | 306.36 | 306.36 | 0.00% | 306.36 | 0.00% |
| Cr105 | 10 | 310.22 | 310.22 | 310.22 | 0.00% | 310.22 | 0.00% |
| Cr106 | 10 | 315.47 | 317.32 | 315.47 | 0.59% | 316.35 | 0.31% |
| Cr107 | 10 | 309.59 | 309.59 | 310.13 | −0.17% | 310.42 | −0.27% |
| Cr108 | 10 | 310.87 | 310.87 | 342.14 | −9.14% | 327.46 | −5.07% |
| Cr201 | 20 | 312.21 | 312.21 | 325.44 | −4.07% | 324.62 | −3.82% |
| Cr202 | 20 | 312.43 | 312.43 | 318.62 | −1.94% | 318.1 | −1.78% |
| Cr203 | 20 | 310.34 | 315.25 | 312.09 | 1.01% | 310.34 | 1.58% |
| Cr204 | 20 | 316.84 | 314.13 | 313.24 | 0.28% | 310.65 | 1.12% |
| Cr501 | 50 | 346.03 | 338.55 | 400.15 | −13.52% | 403.57 | −14.26% |
| Cr502 | 50 | 337.31 | 337.31 | 342.16 | −1.42% | 342.33 | −1.47% |
| Cr503 | 50 | 333.32 | 333.32 | 345.34 | −3.48% | 346.44 | −3.79% |
| Cr504 | 50 | 330.07 | 330.07 | 381.12 | −13.39% | 345.62 | −4.50% |
| Cr1001 | 100 | 644.17 | 644.17 | 653.83 | −1.48% | 643.42 | 0.12% |
| Cr1002 | 100 | 646.98 | 646.98 | 780.24 | −17.08% | 683.72 | −5.37% |
| Cr1003 | 100 | 644.32 | 644.32 | 704.28 | −8.51% | 639.12 | 0.81% |
| Cr1004 | 100 | 657.47 | 657.47 | 678.43 | −3.09% | 676.43 | −2.80% |
| Cr1501 | 150 | 757.42 | 757.42 | 845.53 | −10.42% | 840.86 | −9.92% |
| Cr1502 | 150 | 736.21 | 736.21 | 822.53 | −10.49% | 784.23 | −6.12% |
| Cr1503 | 150 | 753.7 | 753.7 | 840.68 | −10.35% | 756.44 | −0.36% |
| Cr1504 | 150 | 770.36 | 770.36 | 812.34 | −5.17% | 774.18 | −0.49% |
| avg | | 424.70 | 424.85 | 450.19 | −4% | 436.22 | −2% |

As shown in Table 6, ALNS-GA obtains the best results in 25 of the 28 tested instances. The columns "ALNS-GA", "ALNS [45]", and "CAGA [47]" report the total delivery cost by the corresponding algorithms, while "$gap_{ALNS}$ (%)" and "$gap_{CAGA}$ (%)" denote the percentage deviation relative to ALNS-GA.

Compared with ALNS and CAGA, the average cost reductions achieved by ALNS-GA are 4% and 2%, respectively. Since the total delivery cost jointly includes vehicle dispatch cost, vehicle transportation cost, drone transportation cost, and time-window penalty cost, these reductions reflect a more effective coordination of vehicle routing, drone assignment, and service scheduling under weather-constrained conditions. For small-scale instances, the solution differences among the three algorithms are relatively minor. However, as the customer scale increases, the proposed algorithm demonstrates increasingly superior solution quality. In the largest instances, ALNS-GA achieves maximum improvements of 15.39% and 16.11% over ALNS and CAGA, respectively. Overall, the results indicate that the proposed ALNS-GA maintains strong and stable optimization performance across instances of different scales, thereby validating its effectiveness in solving the EVRPDWTW problem.

Based on the performance comparison results, further analysis is conducted on the iterative convergence behavior and the optimal delivery routes obtained by the proposed ALNS-GA. Figure 4 illustrates the optimization process of the proposed algorithm using instances Cr501 and Cr1001 as representative examples. For instance Cr501, the algo-

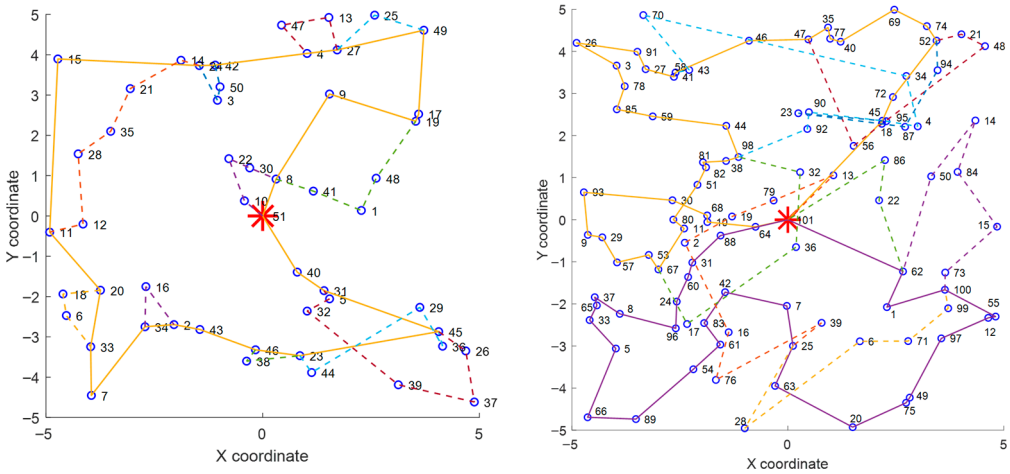
rithm converges after approximately 600 generations, while for the larger instance Cr1001, convergence is achieved after about 700 generations.




(**a**) Cr501 (**b**) Cr1001

**Figure 4.** Diagram of ALNS-GA optimization process.

Figure 5 presents the corresponding optimal routing solutions for Cr501 and Cr1001. In instance Cr501, one vehicle is dispatched, serving 23 customers, while the drone is launched 11 times and serves 27 customers. In instance Cr1001, two vehicles are dispatched, serving 69 customers, and the drone is launched 9 times to serve 31 customers.




(**a**) Cr501 (**b**) Cr1001

**Figure 5.** Delivery routes. Note: The red asterisk denotes the depot, solid lines represent vehicle routes, and dashed lines represent drone routes. Different colors indicate different routes.

### *5.3. Sensitivity Analyses*

To further examine the performance of the proposed framework under different settings, sensitivity analyses are conducted with respect to three factors: the unit distance energy consumption coefficient, the proportion of no-fly periods, and different weather scenarios.

#### 5.3.1. Impact of the Unit Distance Energy Consumption Coefficient

To examine the impact of vehicle energy consumption on system performance, a sensitivity analysis on the unit distance energy consumption coefficient is conducted. Based on previous studies on electric vehicle distribution, three representative energy consumption levels, 1, 1.25, and 1.5 kWh/km, are selected for comparison under the same benchmark instances and algorithm parameter settings. The results are reported in Table 7.

**Table 7.** Comparison of solution results under different energy consumption rates.

| Instance | Customers | Energy Consumption Rate (kWh/km) | | | $Gap_1$ (%) | $Gap_2$ (%) |
|---|---|---|---|---|---|---|
| | | 1.00 | 1.25 | 1.5 | | |
| Cr101 | 10 | 308.06 | 312.63 | 314.77 | 1.48% | 2.18% |
| Cr102 | 10 | 305.56 | 307.94 | 309.38 | 0.78% | 1.25% |
| Cr103 | 10 | 308.39 | 309.44 | 311.03 | 0.34% | 0.86% |
| Cr104 | 10 | 306.36 | 307.21 | 309.32 | 0.28% | 0.97% |
| Cr201 | 20 | 312.21 | 314.82 | 316.55 | 0.84% | 1.39% |
| Cr202 | 20 | 312.43 | 314.53 | 316.42 | 0.67% | 1.28% |
| Cr203 | 20 | 315.25 | 316.39 | 318.25 | 0.36% | 0.95% |
| Cr204 | 20 | 314.13 | 316.85 | 319.17 | 0.87% | 1.60% |
| Cr501 | 50 | 338.55 | 345.99 | 355.76 | 2.20% | 5.08% |
| Cr502 | 50 | 337.31 | 350.54 | 357.82 | 3.92% | 6.08% |
| Cr503 | 50 | 333.32 | 355.38 | 356.37 | 6.62% | 6.92% |
| Cr504 | 50 | 330.07 | 348.51 | 351.48 | 5.59% | 6.49% |
| avg | | 318.47 | 325.02 | 328.03 | 2.00% | 2.92% |

The results show that the total delivery cost increases with the energy consumption coefficient. When the coefficient increases from 1 kWh/km to 1.25 kWh/km, the average cost rises from 318.47 to 325.02. When it further increases to 1.5 kWh/km, the average cost reaches 328.03, representing an increase of 2.92% compared with the baseline case. The effect becomes more pronounced in large-scale instances. For example, the cost increase reaches 6.92% in the Cr503 instance. This indicates that higher energy consumption intensifies vehicle operating costs and encourages shorter routing distances.

#### 5.3.2. Impact of the Proportion of No-Fly Periods

To analyze the effects of the proportion of drone no-fly periods on drone service capability and system operating cost, three no-fly scenarios (Case 1–Case 3) are considered for instances of different scales. In these scenarios, the weather conditions in all non-restricted intervals are kept within the flyable range, so that the analysis focuses specifically on the effect of no-fly duration. The no-fly periods are set to 10:00–12:00, 9:00–13:00, and 9:00–15:00, respectively. The number of drone launches, the number of customers served by drones, and the corresponding total delivery cost are recorded, as summarized in Table 8.

**Table 8.** Comparison of solution results for different flight restriction periods.

| Instance | Customers | Case 1 | | Case 2 | | Case 3 | | $Gap_1$ (%) | $Gap_2$ (%) |
|---|---|---|---|---|---|---|---|---|---|
| | | *D* | *Z* | *D* | *Z* | *D* | *Z* | | |
| Cr103 | 10 | 8 | 311.62 | 8 | 317.36 | 8 | 318.67 | 1.84% | 2.26% |
| Cr202 | 20 | 14 | 315.87 | 14 | 337.23 | 14 | 346.2 | 6.76% | 9.60% |
| Cr504 | 50 | 33 | 336.29 | 32 | 348.04 | 30 | 367.33 | 3.49% | 9.23% |
| Cr1001 | 100 | 42 | 667.17 | 41 | 744.84 | 40 | 804.38 | 11.64% | 20.57% |
| Cr1501 | 150 | 66 | 733.94 | 55 | 876.33 | 43 | 921.41 | 19.40% | 25.54% |
| Avg | | 32.6 | 472.978 | 30 | 524.76 | 27 | 551.598 | 8.63% | 13.44% |

The results indicate that as the duration of no-fly periods increases, the flexibility of drone services is significantly constrained, and a portion of customers must be served exclusively by vehicles. When the no-fly period is extended from 10:00–12:00 to 9:00–15:00, the number of drone launches decreases by 10–20% in some instances, highlighting the substantial impact of weather constraints on task allocation structures. Further analysis reveals that the total cost increases progressively with longer no-fly durations. When the

proportion of no-fly periods increases from 20% to 40% and 60%, the average cost rises by 8.63% and 13.44%, respectively. Moreover, as the customer scale increases, the cost escalation caused by longer no-fly periods becomes more pronounced. For example, in instance Cr1501, the total cost under Case 2 and Case 3 increases by 19.4% and 25.54%, respectively, compared with Case 1.

From a system-level perspective, the increase in no-fly duration leads to a clear reallocation of delivery tasks from drones to vehicles. Under shorter no-fly periods, drones can still undertake a considerable share of geographically dispersed or time-sensitive customers, thereby reducing the travel burden of ground vehicles. However, as the no-fly period expands, the feasible service windows for drones become increasingly limited, and more customers must be reassigned to vehicle routes. This shift weakens the collaborative advantage of the vehicle–drone system and results in longer ground routes, higher vehicle operating costs, and tighter time-window pressure. The effect is particularly pronounced in large-scale instances, where the loss of drone flexibility propagates more strongly through the routing and synchronization structure.

#### 5.3.3. Impact of Different Weather Scenarios

To capture the dynamic characteristics of weather conditions, three scenarios (Case 4–Case 6) are constructed [27]. In these scenarios, the weather state of each time interval is represented by the corresponding wind speed level and no-fly status. In Case 4, the entire delivery period is under ideal weather conditions. In Case 5, ideal weather accounts for 60% of the time horizon, while flight-restricted weather accounts for 40%. In Case 6, ideal weather accounts for 60%, whereas flight-restricted and no-fly weather account for 30% and 10%, respectively. The time horizon is divided into several intervals, and different wind speed levels are assigned to these intervals according to the specified proportions to generate the corresponding wind speed sequences and no-fly indicators. The computational results are presented in Table 9.

**Table 9.** Comparison of solution results under different weather scenarios.

| Instance | Customers | Case 4 | | Case 5 | | Case 6 | |
|---|---|---|---|---|---|---|---|
| | | ***D*** | ***Z*** | ***D*** | ***Z*** | ***D*** | ***Z*** |
| Cr101 | 10 | 8 | 309.22 | 7 | 309.42 | 7 | 313.13 |
| Cr102 | 10 | 8 | 322.43 | 8 | 322.45 | 8 | 324.13 |
| Cr103 | 10 | 7 | 311.61 | 7 | 312.35 | 7 | 315.58 |
| Cr104 | 10 | 9 | 309.54 | 9 | 313.54 | 9 | 320.06 |
| Cr201 | 20 | 15 | 315.87 | 15 | 310.85 | 14 | 348.07 |
| Cr202 | 20 | 16 | 312.18 | 15 | 320.64 | 14 | 369.71 |
| Cr203 | 20 | 16 | 315.97 | 16 | 330.76 | 15 | 372.57 |
| Cr204 | 20 | 14 | 318.13 | 14 | 318.65 | 13 | 360.45 |
| Cr501 | 50 | 27 | 348.51 | 26 | 362.83 | 24 | 388.04 |
| Cr502 | 50 | 37 | 342.24 | 37 | 357.63 | 35 | 390.38 |
| Cr503 | 50 | 37 | 330.64 | 36 | 344.24 | 35 | 365.72 |
| Cr504 | 50 | 36 | 331.75 | 36 | 348.43 | 34 | 374.52 |
| Avg | | 19.17 | 322.34 | 18.83 | 329.32 | 17.92 | 353.53 |

The results show that the number of drone services (D) decreases under different weather conditions. Under ideal weather conditions, the average number of services is 19.17, which decreases to 18.83 and 17.92 in Case 5 and Case 6, respectively. This indicates that increasing weather constraints reduce the number of tasks that drones can perform. In addition, the total cost increases as the duration of no-fly weather grows. The average total

cost (Z) is 322.34 under ideal weather conditions and increases to 329.32 and 353.53 in Case 5 and Case 6, respectively.

A comparison of Case 4, Case 5, and Case 6 reveals that the impact of weather intensity on the delivery system is not purely linear. When the weather changes from ideal conditions to flight-restricted conditions, drone operations remain feasible, and the main effect is a reduction in flight efficiency due to wind-induced travel-time variation. In this stage, the overall service pattern remains largely unchanged, and the cost increase is relatively moderate. By contrast, once no-fly intervals are introduced, the system undergoes a more structural adjustment: some customers that are drone-feasible under milder weather conditions must be reassigned to vehicles, which simultaneously increases vehicle routing burden, reduces drone utilization, and intensifies coordination pressure between ground and aerial delivery resources. Therefore, the increase in total cost under stronger weather scenarios reflects not only lower drone efficiency, but also a fundamental change in task-allocation and routing decisions.

These results indicate that weather intensity affects not only the operational performance of drones, but also the overall coordination mechanism of the vehicle–drone delivery system.

## 6. Conclusions

In this study, the electric vehicle routing problem with drones under weather conditions and time windows (EVRPDWTW) is investigated. A cost-minimization model is developed by jointly considering vehicle dispatch cost, vehicle travel cost, drone flight cost, and time-window penalty cost. The model incorporates weather-dependent drone operations, time-window constraints, and coordinated vehicle–drone delivery decisions within a unified framework.

To solve the proposed problem efficiently, a hybrid ALNS-GA is designed. Computational experiments verify the effectiveness and robustness of the proposed approach and show that it can obtain competitive solutions for both benchmark instances and the constructed EVRPDWTW instances. The results also indicate that the proposed framework is capable of supporting collaborative routing decisions under complex operational constraints.

The sensitivity analysis further shows that weather conditions and vehicle energy consumption significantly affect delivery performance. Under ideal weather, drone participation can be increased to improve efficiency, whereas under flight-restricted or no-fly weather, routing decisions should gradually shift toward more selective or vehicle-dominant delivery strategies. Overall, the proposed framework provides useful support for weather-aware vehicle–drone collaborative delivery planning. Future research may focus on validation with real-world logistics data and the incorporation of more realistic weather uncertainty and UAV energy-consumption mechanisms.

**Author Contributions:** Conceptualization, M.H.; methodology, M.H., X.H. and X.Y.; software, M.H. and X.Y.; validation, M.H., X.Y., X.H. and X.M.; formal analysis, X.Y., X.W. and J.Z.; investigation, M.H., X.Y. and X.M.; resources, M.H., X.H., X.W. and X.M.; data curation, M.H., X.Y., X.W. and J.Z.; writing—original draft, M.H. and X.Y.; writing—review and editing, M.H., X.Y. and X.W.; visualization, X.Y.; supervision, M.H., X.H. and X.W.; project administration, M.H., X.H. and X.W.; funding acquisition, M.H., X.W. and J.Z. All authors have read and agreed to the published version of the manuscript.

**Funding:** This research was funded by the Intelligent Policing Key Laboratory of Sichuan Province (Grant number No. ZNJW2026KFMS002), and Postgraduate Research and Practice Innovation Program of Jiangsu Province (Grant number No. KYCX24_3984).

**Data Availability Statement:** The original contributions presented in the study are included in the article and further inquiries can be directed to the corresponding author.

**Conflicts of Interest:** The authors declare no conflicts of interest.

## References


1. Zhang, G.; Zhang, J.; He, B.; Zhang, R.; Zou, X. An optimisation model of hierarchical facility location problem for urban last-mile delivery with drones. *Transp. A Transp. Sci.* **2024**, *20*, 1–29. [CrossRef]
2. Lee, H.; Lee, C. Research on logistics of intelligent unmanned aerial vehicle integration system. *J. Ind. Inf. Integr.* **2023**, *36*, 100534. [CrossRef]
3. Wang, W.; Adulyasak, Y.; Cordeau, J.; He, G. The heterogeneous-fleet electric vehicle routing problem with nonlinear charging functions. *Transp. Res. Part C Emerg. Technol.* **2025**, *170*, 104932. [CrossRef]
4. Zhang, S.; Liu, S.; Xu, W.; Wang, W. A novel multi-objective optimization model for the vehicle routing problem with drone delivery and dynamic flight endurance. *Comput. Ind. Eng.* **2022**, *173*, 108679. [CrossRef]
5. Bai, X.; Li, B.; Ullah, I.; Wu, Z.; Basheer, S.; Bashir, A.K. Energy-efficient routing for IoT-enabled multi-truck multi-drone pickup and delivery systems. *Appl. Energy* **2025**, *400*, 126546. [CrossRef]
6. Heidari, A.; Raeesi, R.; Mahjouri, N.; Rasti-Barzoki, M. A multi-objective model for cooperative delivery of customer orders using multiple trucks and UAVs considering weather conditions. *Internet Things* **2025**, *31*, 101539. [CrossRef]
7. Schneider, M.; Stenger, A.; Goeke, D. The electric vehicle-routing problem with time windows and recharging stations. *Transp. Sci.* **2014**, *48*, 500–520. [CrossRef]
8. Kucukoglu, I.; Dewil, R.; Cattrysse, D. The electric vehicle routing problem and its variations: A literature review. *Comput. Ind. Eng.* **2021**, *161*, 107650. [CrossRef]
9. Hiermann, G.; Puchinger, J.; Ropke, S.; Hartl, R.F. The Electric Fleet Size and Mix Vehicle Routing Problem with Time Windows and Recharging Stations. *Eur. J. Oper. Res.* **2016**, *252*, 995–1018. [CrossRef]
10. Wang, W.; Zhao, J. Partial linear recharging strategy for the electric fleet size and mix vehicle routing problem with time windows and recharging stations. *Eur. J. Oper. Res.* **2023**, *308*, 929–948. [CrossRef]
11. Souza, A.L.S.; Papini, M.; Penna, P.H.V.; Souza, M.J.F. A flexible variable neighbourhood search algorithm for different variants of the Electric Vehicle Routing Problem. *Comput. Oper. Res.* **2024**, *168*, 106713. [CrossRef]
12. Bruglieri, M.; Paolucci, M.; Pisacane, O. A matheuristic for the electric vehicle routing problem with time windows and a realistic energy consumption model. *Comput. Oper. Res.* **2023**, *157*, 106261. [CrossRef]
13. Rastani, S.; Çatay, B. A large neighborhood search-based matheuristic for the load-dependent electric vehicle routing problem with time windows. *Ann. Oper. Res.* **2023**, *324*, 761–793.
14. Lera-Romero, G.; Miranda Bront, J.J.; Soulignac, F.J. A branch-cut-and-price algorithm for the time-dependent electric vehicle routing problem with time windows. *Eur. J. Oper. Res.* **2024**, *312*, 978–995.
15. Ham, A.M. Integrated scheduling of m-truck, m-drone, and m-depot constrained by time-window, drop-pickup, and m-visit using constraint programming. *Transp. Res. Part C Emerg. Technol.* **2018**, *91*, 1–14.
16. Kitjacharoenchai, P.; Min, B.; Lee, S. Two echelon vehicle routing problem with drones in last mile delivery. *Int. J. Prod. Econ.* **2020**, *225*, 107598. [CrossRef]
17. Huang, S.; Huang, Y.; Blazquez, C.A.; Chen, C. Solving the vehicle routing problem with drone for delivery services using an ant colony optimization algorithm. *Adv. Eng. Inform.* **2022**, *51*, 101536. [CrossRef]
18. Chu, J.C.; Shui, C.S.; Lin, K. Optimization of trucks and drones in tandem delivery network with drone trajectory planning. *Comput. Ind. Eng.* **2024**, *189*, 110000. [CrossRef]
19. Chang, Y.S.; Lee, H.J. Optimal delivery routing with wider drone-delivery areas along a shorter truck-route. *Expert Syst. Appl.* **2018**, *104*, 307–317. [CrossRef]
20. Jeong, H.Y.; Song, B.D.; Lee, S. Truck-drone hybrid delivery routing: Payload-energy dependency and no-fly zones. *Int. J. Prod. Econ.* **2019**, *214*, 220–233. [CrossRef]
21. Karak, A.; Abdelghany, K. The hybrid vehicle-drone routing problem for pick-up and delivery services. *Transp. Res. Part C Emerg. Technol.* **2019**, *102*, 427–449. [CrossRef]
22. Wang, Y.; Wang, Z.; Hu, X.; Xue, G.; Guan, X. Truck-drone hybrid routing problem with time-dependent road travel time. *Transp. Res. Part C Emerg. Technol.* **2022**, *144*, 103901. [CrossRef]
23. Cui, H.; Li, K.; Jia, S.; Meng, Q. Dynamic collaborative truck-drone delivery with en-route synchronization and random requests. *Transp. Res. Part E Logist. Transp. Rev.* **2024**, *192*, 103802. [CrossRef]
24. Kyriakakis, N.A.; Stamadianos, T.; Marinaki, M.; Marinakis, Y. The electric vehicle routing problem with drones: An energy minimization approach for aerial deliveries. *Clean. Logist. Supply Chain* **2022**, *4*, 100041. [CrossRef]

25. Mara, S.T.W.; Sarker, R.; Essam, D.; Elsayed, S. Solving electric vehicle-drone routing problem using memetic algorithm. *Swarm Evol. Comput.* **2023**, *79*, 101295. [CrossRef]
26. Xiao, J.; Li, Y.; Cao, Z.; Xiao, J. Cooperative trucks and drones for rural last-mile delivery with steep roads. *Comput. Ind. Eng.* **2024**, *187*, 109849. [CrossRef]
27. Zhang, S.; Liu, S.; Zhang, W. Vehicle Routing Problem with Time Windows in Electric Vehicle-Drone Collaborative Delivery Mode. *Chin. J. Manag. Sci.* **2025**, *33*, 131–141.
28. Park, Y.; Jeong, J.; Wang, C.; Woo, S. Multi-modal electric logistics system: Electric trucks as floating chargers for electric drones. *Transp. Res. Part D Transp. Environ.* **2025**, *146*, 104843. [CrossRef]
29. Campuzano, G.; Lalla-Ruiz, E.; Mes, M. The drone-assisted variable speed asymmetric traveling salesman problem. *Comput. Ind. Eng.* **2023**, *176*, 109003. [CrossRef]
30. Di Puglia Pugliese, L.; Guerriero, F.; Scutellá, M.G. The last-mile delivery process with trucks and drones under uncertain energy consumption. *J. Optim. Theory Appl.* **2021**, *191*, 31–67. [CrossRef]
31. Dodge, M.; MirHassani, S.A.; Hooshmand, F. A modelling and solution approach for wind-affected drone-truck routing problem under uncertainty. *Expert Syst. Appl.* **2024**, *257*, 124996. [CrossRef]
32. Lu, Y.; Yang, J.; Yang, C. A humanitarian vehicle routing problem synchronized with drones in time-varying weather conditions. *Comput. Ind. Eng.* **2023**, *184*, 109563. [CrossRef]
33. Cheng, C.; Adulyasak, Y.; Rousseau, L.-M. Robust drone delivery with weather information. *Manuf. Serv. Oper. Manag.* **2024**, *26*, 1402–1421. [CrossRef]
34. Ren, X.; Fan, H.; Fan, H.; Ma, M. Time-dependent electric vehicle-drone routing problem for scheduled deliveries and on-demand pickups considering variable drone speeds and no-fly zones. *Comput. Oper. Res.* **2025**, *182*, 107141. [CrossRef]
35. Euchi, J.; Sadok, A. Hybrid genetic-sweep algorithm to solve the vehicle routing problem with drones. *Phys. Commun.* **2021**, *44*, 101236. [CrossRef]
36. Mahmoudinazlou, S.; Kwon, C. A hybrid genetic algorithm with type-aware chromosomes for traveling salesman problems with drone. *Eur. J. Oper. Res.* **2024**, *318*, 719–739. [CrossRef]
37. Wang, Y.; Wang, Z.; Song, M.; Fang, L. Route Optimization of Refrigerated Container Multimodal Transport Under Uncertain Transit Time. *J. Transp. Syst. Eng. Inf. Technol.* **2025**, *25*, 124–134.
38. Fan, H.; Liu, K.; Wang, J.; Zhao, J. Multi-depot electric vehicle routing problem with drones considering time-dependent traffic. *Adv. Eng. Inform.* **2026**, *69*, 104008. [CrossRef]
39. Jia, Y.; Mei, Y.; Zhang, M. A bilevel ant colony optimization algorithm for capacitated electric vehicle routing problem. *IEEE Trans. Cybern.* **2022**, *52*, 10855–10868. [CrossRef]
40. Hesam Sadati, M.E.; Çatay, B.; Aksen, D. An efficient variable neighborhood search with tabu shaking for a class of multi-depot vehicle routing problems. *Comput. Oper. Res.* **2021**, *133*, 105269. [CrossRef]
41. Meng, S.; Chen, Y.; Li, D. The multi-visit drone-assisted pickup and delivery problem with time windows. *Eur. J. Oper. Res.* **2024**, *314*, 685–702. [CrossRef]
42. Ren, X.; Froger, A.; Jabali, O.; Liang, G. A competitive heuristic algorithm for vehicle routing problems with drones. *Eur. J. Oper. Res.* **2024**, *318*, 469–485. [CrossRef]
43. Jiang, J.; Dai, Y.; Yang, F.; Ma, Z. A multi-visit flexible-docking vehicle routing problem with drones for simultaneous pickup and delivery services. *Eur. J. Oper. Res.* **2024**, *312*, 125–137. [CrossRef]
44. Schermer, D.; Moeini, M.; Wendt, O. A hybrid vns/tabu search algorithm for solving the vehicle routing problem with drones and en route operations. *Comput. Oper. Res.* **2019**, *109*, 134–158. [CrossRef]
45. Sacramento, D.; Pisinger, D.; Ropke, S. An adaptive large neighborhood search metaheuristic for the vehicle routing problem with drones. *Transp. Res. Part C Emerg. Technol.* **2019**, *102*, 289–315.
46. Lei, Y.; Huang, Y.; Wang, H. Effects of wind disturbance on the aerodynamic performance of a quadrotor mav during hovering. *J. Sens.* **2021**, *2021*, 6681716.
47. Li, K.; Cui, H.; Meng, Q.; Zhang, X. Dynamic truck-drone collaborative transportation during hurricanes. *Transp. Res. Part C Emerg. Technol.* **2025**, *180*, 105322. [CrossRef]
48. Stodola, P.; Kutěj, L. Multi-depot vehicle routing problem with drones: Mathematical formulation, solution algorithm and experiments. *Expert Syst. Appl.* **2024**, *241*, 122483. [CrossRef]
49. Ribeiro, R.G.; Cota, L.P.; Euzebio, T.A.M.; Ramirez, J.A.; Guimaraes, F.G. Unmanned-aerial-vehicle routing problem with mobile charging stations for assisting search and rescue missions in postdisaster scenarios. *IEEE Trans. Syst. Man Cybern. Syst.* **2022**, *52*, 6682–6696. [CrossRef]


**Disclaimer/Publisher's Note:** The statements, opinions and data contained in all publications are solely those of the individual author(s) and contributor(s) and not of MDPI and/or the editor(s). MDPI and/or the editor(s) disclaim responsibility for any injury to people or property resulting from any ideas, methods, instructions or products referred to in the content.